VIETNAM NATIONAL UNIVERSITY, HANOI
UNIVERSITY OF SCIENCE

.

Pham The An

IMPROVEMENTS OF CRITICAL CURRENT DENSITY OF Bi-Pb-Sr-Ca-Cu-O HIGH-T_c SUPERCONDUCTOR BY ADDITIONS OF NANO-STRUCTURED PINNING CENTERS

Major: Thermophysics
Code: 9440130.07

DISSERTATION SUMMARY FOR DOCTOR OF PHILOSOPHY IN PHYSICS

Ha Noi – 2023

The work was completed at: University of Science, Vietnam National University, Hanoi

Supervisors: Prof. Dr. Luu Tuan Tai, Assoc. Prof. Dr. Tran Hai Duc

Reviewer: Prof.Dr. Nguyen Huy Dan, Institute of Materials Science, Vietnam Academy of Science and Technology

Reviewer: Prof.Dr. Nguyen Phuc Duong, School of Materials Science and Engineering, Hanoi University of Science and Technology

Reviewer: Assoc.Prof.Dr. Ho Khac Hieu, Duy Tan University

The dissertation was defended before the Dissertation Evaluation Council meeting at the University of Science, Vietnam National University, Hanoi at 3:00 PM on December 1st, 2023.

The dissertation can be studied at:

- National Library of Vietnam;

- Library and Digital Knowledge Center, Vietnam National University, Hanoi

ABSTRACT

The objective of this dissertation is to systematically investigate the impact of pinning center additions on the enhancement of the critical current density (J_c) and the flux pinning mechanism improvements in $Bi_{1.6}Pb_{0.4}Sr_2Ca_2Cu_3O_{10+\delta}$ polycrystalline superconductors. Specifically, $Bi_{1.6}Pb_{0.4}Sr_2Ca_2Cu_3O_{10+\delta}$ polycrystalline superconductors were synthesized using conventional solid state reaction methods, and the collective pinning theory was applied to gain insight into intrinsic pinning properties and improvements to J_c in the Bi-Pb-Sr-Ca-Cu-O (BPSCCO) system. This dissertation presents an investigation into the J_c and pinning mechanism in BPSCCO superconductors. Additionally, various types of nano-sized pinning centers, including point-like defects, non-magnetic, and magnetic nanoparticles, were added to BPSCCO samples to further investigate their effects.

CHAPTER 1: OVERVIEW

1.1. INTRODUCTION

1.1.1. History of Superconductivity

The study of superconductivity has led to many important discoveries in the field of condensed matter physics, and it continues to be an active area of research for scientists around the world.

1.1.2. Critical parameters of a superconductor

J_c is an important critical parameter for electric transport and magnetic field generate.

1.1.3. Superconductor classification

Type-II superconductor is a high applicability material featured by B_{c2} and flux pinning phenomena. The study of J_c and vortices in high-T_c

(a type-II group of type-II superconductor with T_c > 77 K) superconductor is an active area of research and potential.

1.2. VORTEX DYNAMICS IN TYPE-II SUPERCONDUCTORS

The collective pinning theory is the effective theory described vortices behavior and pinning mechanism in high-T_c superconductor and were applied widely in cuprated superconductor. The Dew-Hughes model for flux pinning mechanism in type-II superconductor was applied on this dissertation by consider the type of interaction, type of pinning center and pinning center geometry.

1.3. RECENT STUDIES ON THE FIRST GENERATION SUPERCONDUCTING WIRE

Bi-Sr-Ca-Cu-O (BSCCO) high-temperature superconductor superconductors have been considered to be promising materials for industrial applications. Usual superconducting phase in the BSCOO bulk: Bi-2201, Bi-2212 and Bi-2223 are ~ 20 K, 80 K, and 110 K, respectively. In this dissertation, the ratio of Bi:Pb was maintained as 1.6:0.4, which was found to be the optimum ratio for obtaining the highest $T_{c.}$ Studies on applications of BSCCO have been focused on improve J_c and B_{c2}. Additions of nanostructured pinning centers have been proved to be effective to achieve the high J_c and B_{c2} in BSCCO superconductors at measurement temperatures with the microscopic theories.

1.4. MOTIVATION OF THE DISSERTATION

The systematic investigations of enhancements of J_c and detailed analyses on flux pinning mechanism in BSCCO with the additions of nanostructured pinning centers are going to be carried out. Different types of nanostructured pinning centers have been introduced sepa-

rately into BSCCO. Collective pinning theory and Dew -Hughes models are going to be applied to examine the pinning mechanism, geometry of pinning centers to give insight in the origins of enhancements of J_c.

CHAPTER 2: EXPERIMENTS

2.1. SAMPLE FABRICATIONS

2.1.1 Fabrication of Bi-Pb-Sr-Ca-Cu-O polycrystalline samples

The sample of stoichiometry of $Bi_{1.6}Pb_{0.4}Sr_2Ca_2Cu_3O_{10+\delta}$ were prepared by the conventional solid-state reaction technique.

2.1.2. Fabrication of nanoparticles

Semiconducting TiO_2 nanoparticles were prepared by the hydrothermal route.

Magnetic Fe_3O_4 nanoparticles were synthesized by the chemical co-precipitation route.

2.1.3. Introductions of pinning centers into Bi-Pb-Sr-Ca-Cu-O polycrystalline samples

The completed fabrication process was illustrated in Figure. 2.1.

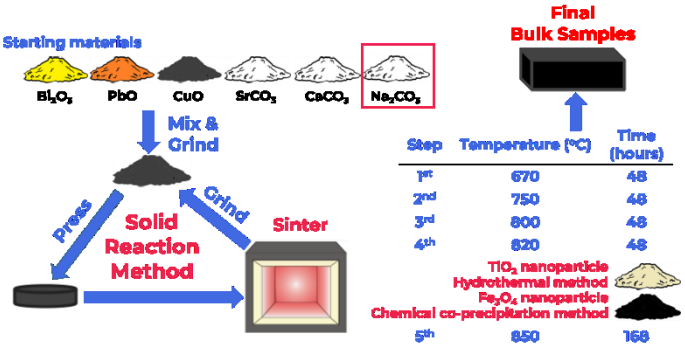

Figure 2.1. Fabrication process of sample series illustration

2.2. SAMPLE CHARACTERIZATIONS

Samples were characterized by TEM, XRD, SEM, XAS, four-probe and PPMS measurements.

CHAPTER 3: IMPROVEMENTS OF CRITICAL CURRENT DENSITY IN HIGH-T_c $Bi_{1.6}Pb_{0.4}Sr_2Ca_2Cu_3O_{10+\delta}$ OF SUPERCONDUCTOR BY USING SODIUM SUBSTITUTION EFFECT

3.1. FORMATION OF THE SUPERCONDUCTING PHASES

All fabricated samples clearly showed the formation of Bi-2223 and Bi-2212 superconducting phases. No impurity phase was detected.

3.2. IMPROVEMENTS OF J_c

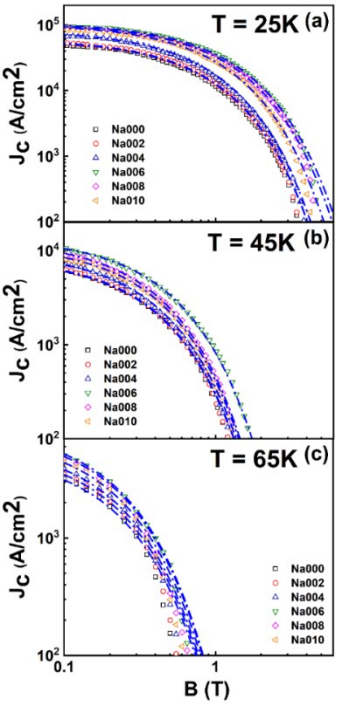

Figure 3.4. Descriptions of the field dependence of J_c of all samples by using the collective pinning theory at (a) 65 K, (b) 45K and (c) 25

K. The solid lines are the fitting curves using Eq. (1.2)

The J_c was enhanced from Na002, reached a maximum at Na006, and then decreased for Na008 and Na010 samples. The enlargements of single vortex pinning, and small bundle pinning regions would attribute to the enhancements of the flux pinning properties in the Na006 sample, which were provided by Na substitution.

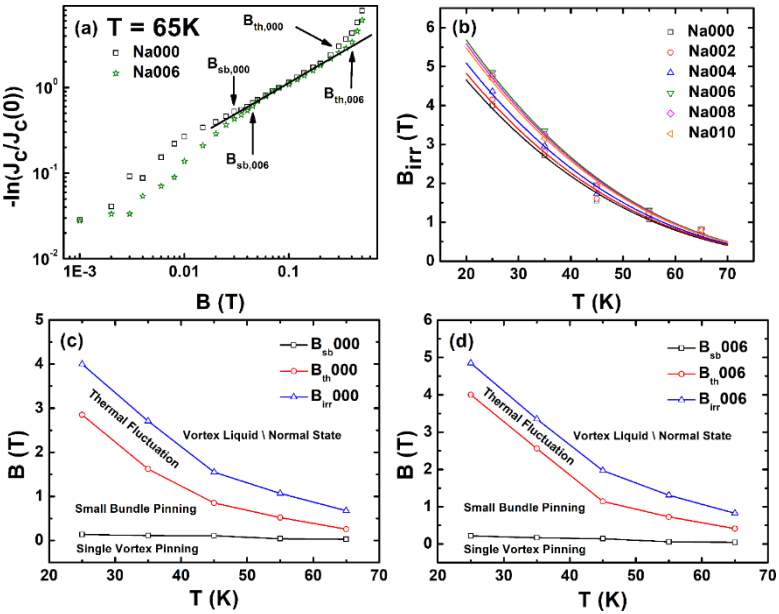

Figure 3.5. (a) Field dependence of -ln($J_c(B)/J_c(0)$) of Na000 and Na006 samples at 65K. (b) The temperature dependence of B_{irr} of all samples at different temperatures. The solid lines are the fitting curves using Eq. (3.1). (c) The B-T phase diagram of Na000 sample. (d) The B-T phase diagram of Na006 sample

3.3. FLUX PINNING PROPERTIES

In Figure 3.8, the maximum p and q were achieved on Na006 sample, which are 0.70 and 1.92, respectively revealing that the core interaction was the predominant pinning mechanism in all samples. The formation of 0D point like defects created by the partial Na substitution has been shown to provide J_c enhancement. In Figure 3.9, results of fitting $J_c/J_c(0)$ and B_{sb} vs. t using the collective pining theory indicate that the δl pinning was dominant in a wide range of temperature and fields.

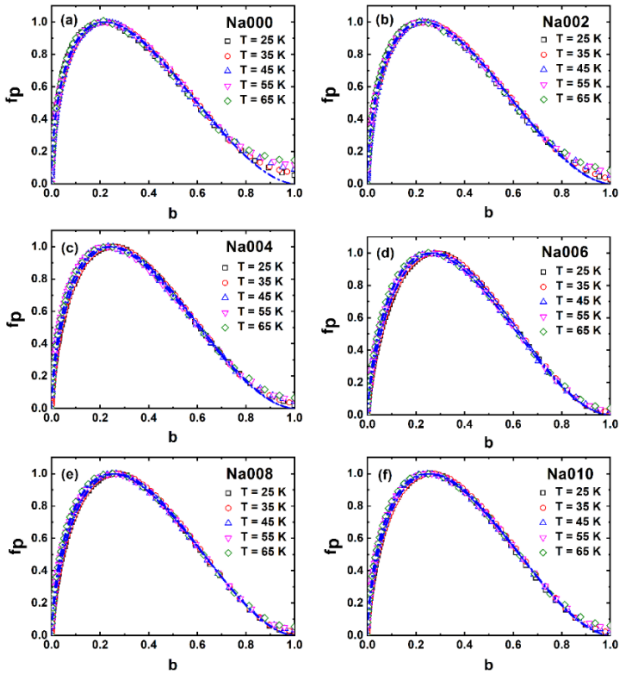

Figure 3.8. Scaling behaviors at all measured temperatures of (a) Na000, (b) Na002, (c) Na004, (d) Na006, (e) Na008 and (f) Na010 samples. The solid lines are the fitting curves using Eq. (1.7).

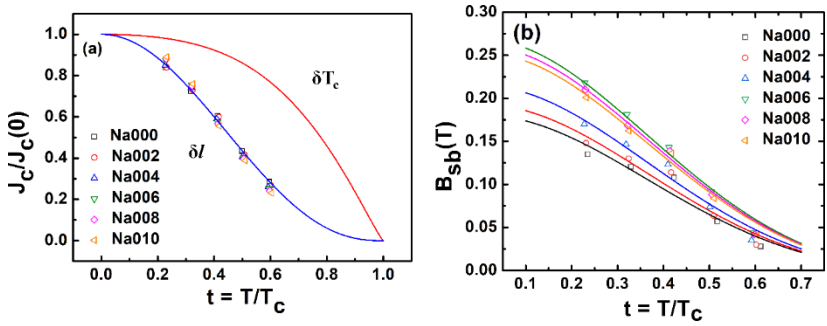

Figure 3.9. (a) Normalized critical current density $J_c(t)/J_c(0)$ versus normalized temperature t of all the samples; (b) Crossover field (B_{sb}) versus normalized temperature of all the samples. The solid lines are the fitting curves using Eq. 1.5.

3.4. CONCLUSION OF CHAPTER 3

In this chapter, the scaling behaviour of flux pinning forces in $Bi_{1.6}Pb_{0.4}Sr_2Ca_{2-x}Na_xCu_3O_{10+\delta}$ superconductors was systematically investigated. It was found that the magnetic field dependence of J_c at different temperatures ranged between 65 K and 25 K was significantly enhanced by the Na substitution via point-like defect creations. This field dependence of J_c was well described using the collective pinning theory. The B-T phase diagrams were constructed. The improved flux pinning properties in the Na-substituted samples were evident from comparing the fitting values of p, q and b_{peak} following the Dew-Hughes model.

CHAPTER 4: IMPROVEMENTS OF CRITICAL CURRENT DENSITY IN HIGH-T_c $Bi_{1.6}Pb_{0.4}Sr_2Ca_2Cu_3O_{10+\delta}$ SUPERCONDUCTOR BY ADDITION OF NON-MAGNETIC TiO_2 NANOPARTICLES

4.1. NANOPARTICLE CHARACTERISTICS

The average size of the TiO_2 nanoparticles was around 12 nm as examined by using TEM image.

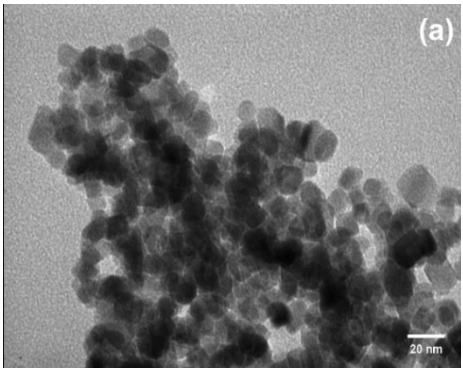

Figure 4.1. (a) TEM images of TiO_2 nanoparticles

4.2. FORMATION OF THE SUPERCONDUCTING PHASES

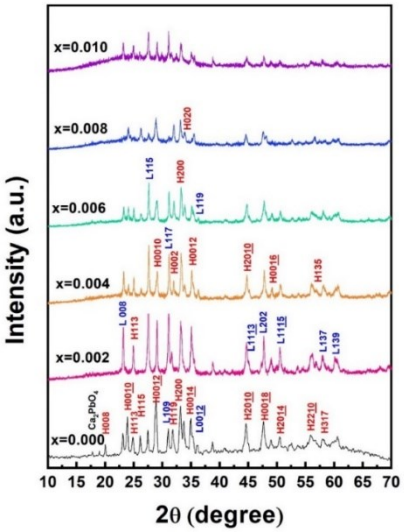

Figure 4.2. XRD patterns of $(Bi_{1.6}Pb_{0.4}Sr_2Ca_2Cu_3O_{10+\delta})_{1-x}(TiO_2)_x$ samples, with x = 0, 0.002, 0.004, 0.006, 0.008, and 0.0104.

The volume fraction values showed that *%Bi-2223* was decreased, whereas *%Bi-2212* was increased monotonously by increasing the TiO_2 content. The volume fraction and crystallite size investigation results revealed that TiO_2 nanoparticle decelerated Bi-2223 phase formation. The lattice parameters were around $a = b = 5.395 \pm 0.007$ Å and $c = 37.07 \pm 0.01$ Å relating to the tetragonal structure.

4.3. THE CORRELATION BETWEEN LOCAL STRUCTURE VARIATIONS AND CRITICAL TEMPERATURE

4.3.1. Critical temperature

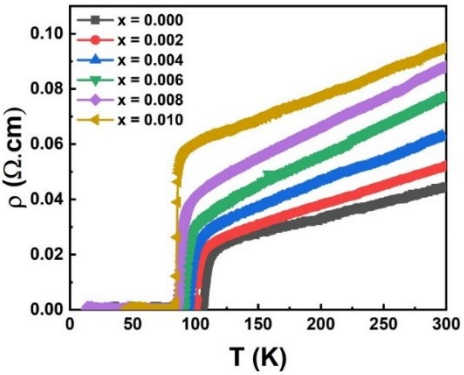

Figure 4.4. The temperature dependence of resistivity of $(Bi_{1.6}Pb_{0.4}Sr_2Ca_2Cu_3O_{10+\delta})_{1-x}(TiO_2)_x$ samples, with x = 0, 0.002, 0.004, 0.006, 0.008, and 0.010

Superconducting transitions were observed in all samples. The T_c of the samples was decreased by the addition of TiO_2. The ρ_0 is increased gradually with x = 0.002, 0.004. From x = 0.006, the value of ρ_0 increases more strongly; when x = 0.010, the ρ_0 is about thrice higher

than that in the pure sample.

4.3.2. Fluctuation of mean field region

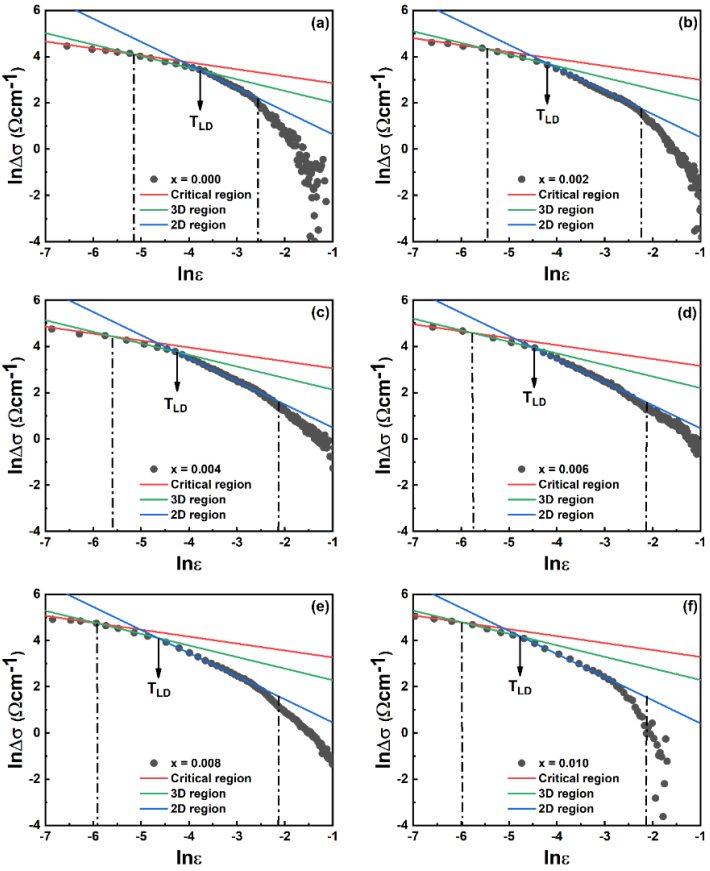

Figure 4.5. Double logarithmic plot of excess conductivity as a function of reduced temperature of $(Bi_{1.6}Pb_{0.4}Sr_2Ca_2Cu_3O_{10+\delta})_{1-x}(TiO_2)_x$ samples (a) $x = 0$, (b) $x = 0.002$, (c) $x = 0.004$, (d) $x = 0.006$, (e) $x = 0.008$, and (f) $x = 0.010$. The red, green, and blue solid lines correspond to the critical region, 3D and 2D region, respectively

From Figure 4.4, the coherence length and effective inter-layering spacing were estimated and found to increase with increasing doping content. This result explains the reduction in the superconducting properties of the material in the CuO_2 interlayer.

4.3.3. Local structure variations

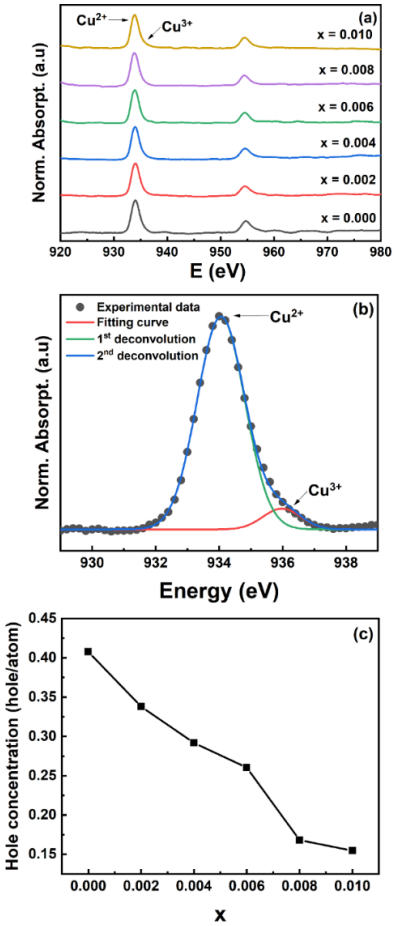

Figure 4.8. (a) Cu K-edge XANES spectra of

$(Bi_{1.6}Pb_{0.4}Sr_2Ca_2Cu_3O_{10+\delta})_{1-x}(TiO_2)_x$ samples, with x = 0, 0.002, 0.004, 0.006, 0.008, and 0.010. (b) Copper valence of all samples

The Cu $L_{2,3}$-edge spectra for all samples are plotted in Figure 4.5(a). The carrier concentration in the conducting planes was calculated from the XANES spectra of Cu $L_{2,3}$-edge. Two main peaks appeared at approximately 933 and 955 eV for all samples. In Figure 4.5(b) the pseudo-Voigt function was used to fit L_3 peaks to find the ratio of Cu2+ to Cu3+, which led to the estimation of hole concentration (p). p was obtained to decrease as increasing the addition level of TiO_2 as given in Figure 4.5(c), which would be evidenced for the observed degradation of T_c.

4.4. IMPROVEMENTS OF J_c

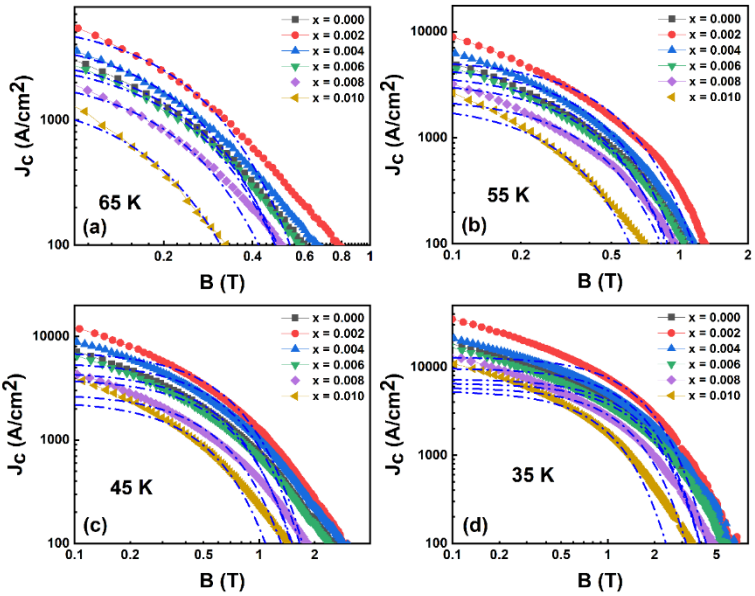

Figure 4.10. The field dependence of J_c of $(Bi_{1.6}Pb_{0.4}Sr_2Ca_2Cu_3O_{10+\delta})_{1-x}(TiO_2)_x$ samples, with x = 0, 0.002,

0.004, 0.006, 0.008, and 0.010 at (a) 65 K, (b) 55 K, (c) 45 K, and (d) 35 K. Dash-dot lines are fitting curves of collective pinning theory.

J_c enhancements were obtained at a dopant amount of $x = 0.002$ and $x = 0.004$ samples. Furthermore, when all samples were compared, J_c descended much slower under the applied field on these samples. conditions with the proper amount of doping content.

First, in the single vortex regime, where the vortices are individually pinned, the J_c in field is nearly plateau. On $x = 0.002$ and $x = 0.004$, the plateau J_c was wider, which could prove the increment in pinning center quantity. With increasing magnetic field, the vortex density became greater than the pinning center density. Therefore, the extension of both the single vortex and collective pinning regimes was probably indicated by the appearance of additional nano-defects as additional pinning centers. These artificial pinning centers also revealed a good collective pinning ability via the extension of the small bundle regime.

4.5. FLUX PINNING PROPERTIES

4.5.1. Flux pinning mechanism

The natural pinning center is defined as grain boundaries on the pure sample, and δl pinning is reasonable for this type of center. In Figure 4.7, results of fitting $J_c/J_c(0)$ and $B_{sb}/B_{sb}(0)$ vs. t using the collective

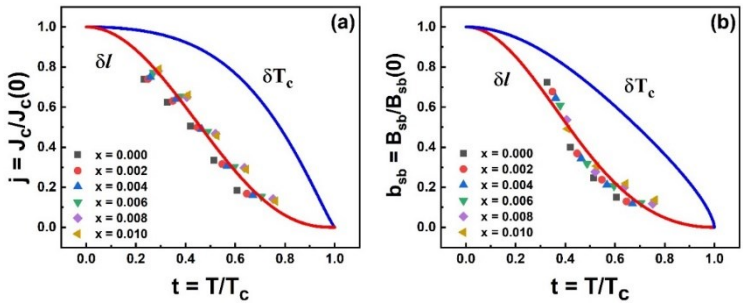

pining theory indicate that the δl pinning was dominant in a wide range of temperature and fields..

Figure 4.11. (a) The normalized temperature dependence of normalized J_c and (b) normalized B_{sb} of $(Bi_{1.6}Pb_{0.4}Sr_2Ca_2Cu_3O_{10+\delta})_{1-x}(TiO_2)_x$ samples, with x = 0, 0.002, 0.004, 0.006, 0.008, and 0.010. Solid lines are fitting curves in terms of the δl pinning and δT_c pinning mechanisms.

4.5.3. Identification of flux pinning center

Compared with the inter-flux-line spacing $d = 1.07(\Phi_0/B)^{1/2}$, the average size of TiO_2 nanoparticles was smaller than that in all investigated range of magnetic field. Therefore, the geometry of center was satisfied as point-like pinning center. Hence, the doped TiO2 nanoparticles operated as the normal core point pinning centers on doped samples,

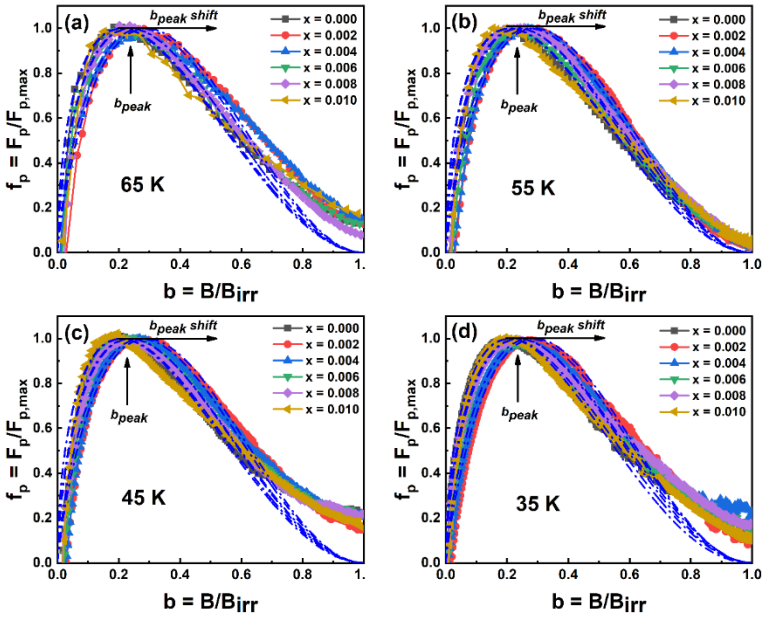

corresponding to $p = 1$ and $q = 2$ in Dew-Hughes's model.

Figure 4.13. The normalized field dependence of $(Bi_{1.6}Pb_{0.4}Sr_2Ca_2Cu_3O_{10+\delta})_{1-x}(TiO_2)_x$ samples, with $x = 0$, 0.002, 0.004, 0.006, 0.008, and 0.010 with modified Dew-Hughes model scaling at (a) 65 K, (b) 55 K, (c) 45 K ,and (d) 35 K. Solid lines are fitting curves using Eq. 1.7.

4.6. CONCLUSION OF CHAPTER 4

The effects of TiO_2 nanoparticles on the structure, morphology, critical and flux pinning properties of $Bi_{1.6}Pb_{0.4}Sr_2Ca_2Cu_3O_{10+\delta}$ superconductor were systematically investigated. The excess conductivity in the framework of the A–L and L–D theory analyses displayed that the mean field region was fluctuated by TiO_2 with increasing c-axis coherence length and effective CuO_2 interlayer spacing. The reduction in both Cu valence state and hole concentration on the doped sample was probed by using Cu K-edge and Cu $L_{2,3}$-edge XANES spectra. The $J_c(B)$ of the samples were enhanced by adequate doping contents of $x = 0.002$, 0.004. The values of B_{sb} and B_{lb} were estimated for all samples at 65, 55, 45, and 35 K. The results revealed the extension of the small and large bundle regimes with adequate amounts of TiO_2 nanoparticles. The $j(t)$ analyses exhibited that the δl pinning was the dominant pinning mechanism in all samples. The increasing p fitting parameter increase on $x = 0.002$ and 0.004 samples exhibited that the additional centers were normal core point pinning centers.

CHAPTER 5: IMPROVEMENTS OF CRITICAL CURRENT DENSITY IN HIGH-T_c $Bi_{1.6}Pb_{0.4}Sr_2Ca_2Cu_3O_{10+\delta}$ SUPERCONDUCTOR BY ADDITION OF MAGNETIC Fe_3O_4 NANOPARTICLES

5.1. NANOPARTICLE CHARACTERISTICS

The nanoparticles were found to be mostly in spherical form and its average size was about 19 nm as evidenced via the TEM image (not shown here).

5.2. FORMATION OF THE SUPERCONDUCTING PHASES

The %Bi-2223 phase monotonously decreased, whereas the %Bi-2212 phase increased with the increase in addition. The average crystallite size continuously decreased. Fe_3O_4 nanoparticles possibly decelerated the Bi-2223 formation.

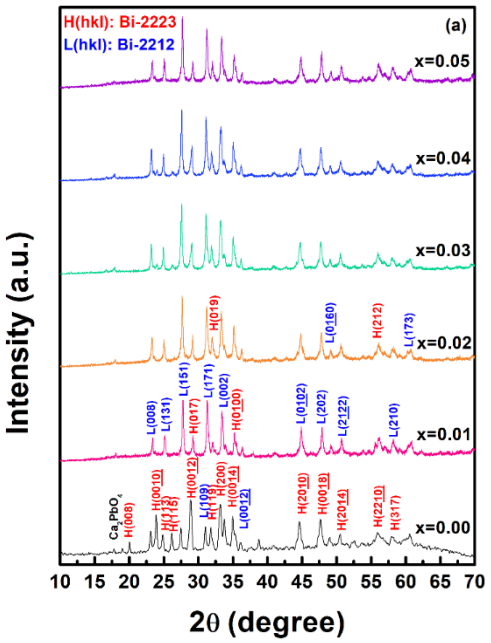

Figure 5.2. (a) XRD patterns of $(Bi_{1.6}Pb_{0.4}Sr_2Ca_2Cu_3O_{10+\delta})_{1-x}(Fe_3O_4)_x$ samples, with x = 0, 0.01, 0.02, 0.03, 0.04, and 0.05

5.3. IMPROVEMENTS OF J_c

The results revealed that the J_c values of the doped samples increased for x = 0.01 and 0.02 and gradually decreased for $x \geq 0.03$. The strongest J_c enhancement was obtained on the $x = 0.02$ sample.

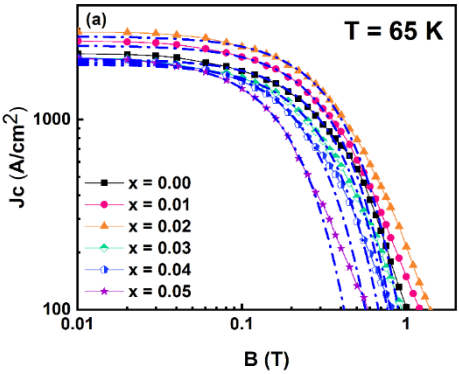

Figure 5.4. (a) Field dependence of J_c at 65 K with small-bundle regime fitting in double-logarithmic scale of the x = 0 and 0.02 samples

5.4. FLUX PINNING PROPERTIES

5.4.1. Identification of pinning center

For the x = 0.01 and 0.02 samples, the value of p increased from

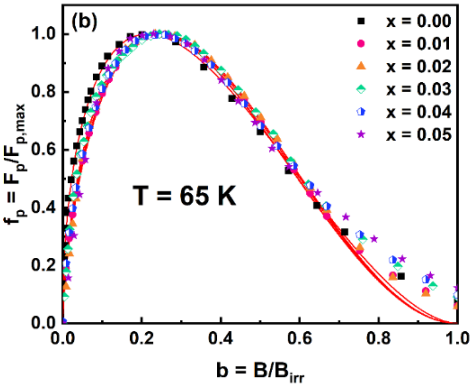

0.5537 to 0.6523 and 0.6695, and the value of b_{peak} increased from 0.2168 to 0.2459 and 0.2508, respectively, with both exhibiting the point-like pinning mechanism (b_{peak} = 1/3).

Figure 5.5. (a) Normalized field dependence of F_p at 65 K, (b) normalized field dependence of f_p with Dew–Hughes model fitting of $(Bi_{1.6}Pb_{0.4}Sr_2Ca_2Cu_3O_{10+\delta})_{1-x}(Fe_3O_4)_x$ samples, with x = 0, 0.01, 0.02, 0.03, 0.04, and 0.05

5.4.2. Improvements of pinning potential

The precipitates at grain boundaries improve U_0 of Bi-2212 bulks. Possible reasons for the enhancements were attributed to: (i) the improved pinning force F_p and (ii) and strengthened activation energy U_0.

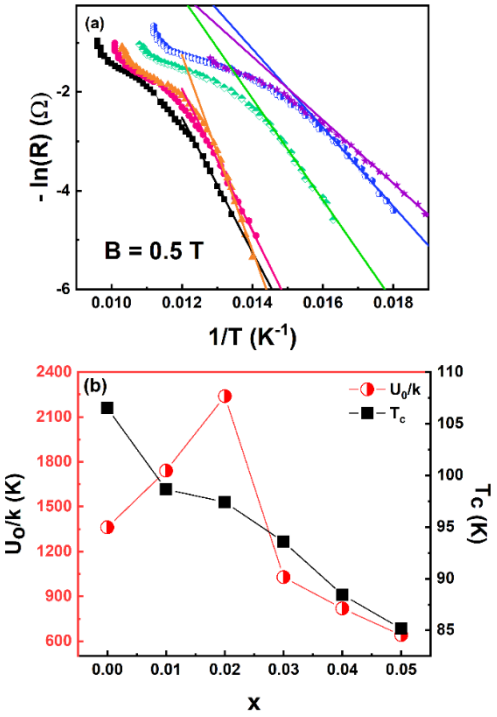

Figure 5.6. (a) Arrhenius plot at 0.5T using Equation (5.1), and (b) Pinning potential and T_c of $(Bi_{1.6}Pb_{0.4}Sr_2Ca_2Cu_3O_{10+\delta})_{1-x}(Fe_3O_4)_x$ samples, with x = 0, 0.01, 0.02, 0.03, 0.04, and 0.05

5.5. COMPARISON OF SUBSTITUTION EFFECT, NON-MAGNETIC AND MAGNETIC NANOPARTICLES DOPING ON THE CRITICAL CURRENT DENSITY OF $Bi_{1.6}Pb_{0.4}Sr_2Ca_2Cu_3O_{10+\delta}$ CERAMIC SUPERCONDUCTOR

The results illustrate that the highest enhancement of J_c was achieved by the addition of Fe_3O_4 magnetic nanoparticles with $x = 0.02$.

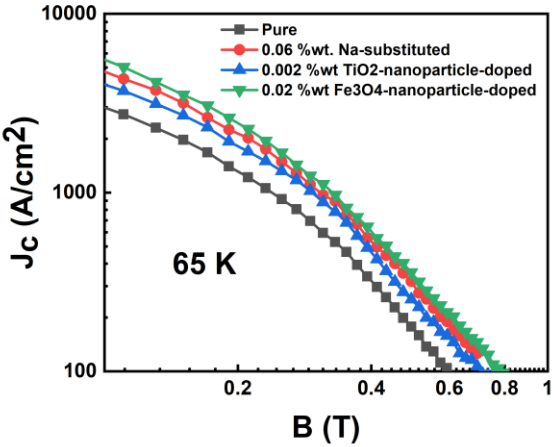

Figure 5.7. The field dependence of J_c at the optimal content of Na-substituted, TiO_2-nanoparticle-doped, and Fe_3O_4-nanoparticle-doped $Bi_{1.6}Pb_{0.4}Sr_2Ca_2Cu_3O_{10+\delta}$ superconductor

CONCLUSIONS

In this dissertation, the explorations of issue of critical current density and pinning mechanism in Bi-Pb-Sr-Ca-Cu-O superconductors were carried out. Main results of this dissertation, improvements of J_c in BPSCCO superconductors, might be summarized as the followings:

The improved flux pinning properties in the Na-substituted samples were evident from comparing the fitting values of p, q and b_{peak} following the Dew-Hughes model. The obtained data also demonstrated the growth of point-like pinning and the decline of grain boundary pinning resulting from the Na substitution. Especially, the δl pinning was found to be the predominant pinning mechanism responsible for the samples, which was related to spatial variations in the mean free path of charge carriers.

For the BPSCCO superconductors with the addition of non-magnetic

TiO_2 nanoparticles, the $J_c(B)$ of the samples were enhanced by adequate doping contents of x = 0.002, 0.004. The results revealed the extension of the small and large bundle regimes with adequate amounts of TiO_2 nanoparticles. The $j(t)$ analyses exhibited that the δl pinning was the dominant pinning mechanism in all samples. The increasing p fitting parameter increase on x = 0.002 and 0.004 samples exhibited that the additional centers were normal core point pinning centers. Additionally, a close correlation between local structural variations and change in T_c of the BPSCCO was investigated. The reduction in both Cu valence state and hole concentration on the doped sample probed by using Cu K-edge and Cu $L_{2,3}$-edge XANES spectra was probably attributed to the observed decrease in T_c of the nanoparticle added BPSCCO superconductors.

For the BPSCCO samples with the additions of magnetic Fe_3O_4 nanoparticles, the enhancements of J_c were obtained for x = 0.01 and 0.02. Possible reasons for the enhancements were attributed to: (i) the improved pinning force and (ii) and strengthened activation energy. Interestingly, the additions of magnetic nanoparticles were concluded to provide the strongest enhancements of J_c among the methods used in the research.

DISSERTATION PUBLICATIONS

[1] **An T. Pham**, Dzung T. Tran, Duong B. Tran, Luu T. Tai, Nguyen K. Man, Nguyen T. M. Hong, Tien M. Le, Duong Pham, Won-Nam Kang, Duc H. Tran (2021), Journal of Electronics Materials 50, pp. 1444-1451.

[2] Dzung T. Tran, **An T. Pham**, Ha H. Pham, Nhung T. Nguyen, Nguyen H. Nam, Nguyen K. Man, Won-Nam Kang, I-Jui Hsu, Wantana Klysubun, Duc H. Tran (2021), Ceramics International 47(12), pp. 16950-16955.

[3] **An T. Pham**, Dzung T. Tran, Ha H. Pham, Nguyen H. Nam, Luu T. Tai, Duc H. Tran (2021), Materials Letters 298, pp. 130015(1-5).

[4] **An T. Pham**, Dzung T. Tran, Linh H. Vu, Nang T.T. Chu, Nguyen Duy Thien, Nguyen H. Nam, Nguyen Thanh Binh, Luu T. Tai, Nguyen T.M. Hong, Nguyen Thanh Long, Duc H. Tran (2022), Ceramics International 48(14), pp. 20996–21004.

[5] **An T. Pham**, Linh H. Vu, Dzung T. Tran, Nguyen Duy Thien, Wantana Klysubun, T. Miyanaga, Nguyen K. Man, Nhan T.T. Duong, Nguyen Thanh Long, Phong V. Pham, Nguyen Thanh Binh, Duc H. Tran (2023), Ceramics International 49(7), pp. 10506-10512.

[6] Tran Tien Dung, **Pham The An**, Tran Ba Duong, Nguyen Khac Man, Nguyen Thi Minh Hien, Tran Hai Duc (2021), VNU Journal of Science: Mathematics – Physics 37(4), pp. 1-10.

[7] **An T. Pham**, Thao V. Nguyen, Yen T. Pham, Duc H. Tran, Nguyen K. Man, Dang T. B. Hop (2019), Proceedings of The 4th International Conference on Advanced Materials and Nanotechnology, pp. 17-20.

[8] **An T. Pham**, Duc V. Ngo, Duc H. Tran, Nguyen K. Man, Dang T. B. Hop (2019), Proceedings of The 4th International Conference on Advanced Materials and Nanotechnology, pp. 36-39.

[9] **An T. Pham**, Dzung T. Tran, Luu T. Tai, Nhung T. Nguyen, Nguyen K. Man, Dang T. B. Hop, Phung Manh Thang, Duc H. Tran (2022), Proceedings of The 12th Vietnam National Conference of Solid Physics and Materials Science, pp. 19-22.